

Tuning the quantum oscillations of surface Dirac electrons in the topological insulator $\text{Bi}_2\text{Te}_2\text{Se}$ by liquid gating.

Jun Xiong¹, Yuehaw Khoo¹, Shuang Jia², R. J. Cava² and N. P. Ong¹

Department of Physics¹ and Department of Chemistry², Princeton University, Princeton, NJ 08544

(Dated: December 11, 2018)

In $\text{Bi}_2\text{Te}_2\text{Se}$, the period of quantum oscillations arising from Dirac surface electrons can be increased 6-fold using ionic liquid gating. At large gate voltages, the Fermi energy reaches the $N = 1$ Landau level in a 14-Tesla field. This enables the $\frac{1}{2}$ -shift predicted for the Dirac spectrum to be measured accurately. A surprising result is that liquid gating strongly enhances the surface mobility. By analyzing the Hall conductivity, we show that the enhancement occurs on only one surface.

PACS numbers: 72.15.Rn, 03.65.Vf, 71.70.Ej, 73.25.+i

A Topological Insulator (TI) is characterized by the existence of current-carrying surface states that traverse the bulk energy gap [1, 2]. There is strong interest in the helical nature of the surface states, which results from the locking of the electron's spin transverse to its momentum. In the bismuth-based TI materials, photoemission spectroscopy [3] and scanning tunneling microscopy (STM) [4] have confirmed the spin-locking feature. In transport experiments, the surface states have been detected by surface Shubnikov de Haas (SdH) oscillations in Bi_2Te_3 [5] and $(\text{Bi,Sb})_2\text{Se}_3$ [6], and by Aharonov-Bohm oscillations in Bi_2Se_3 nanowires [7].

Among the Bi-based TI materials, $\text{Bi}_2\text{Te}_2\text{Se}$ currently displays the highest bulk resistivities ($\rho = 1 - 6 \, \Omega\text{cm}$ at 4 K) [8–11]. Despite the large ρ , SdH oscillations may be tracked to temperatures T as high as 38 K [9]. A persistent problem, however, is that the surface Fermi energy E_F in as-grown crystals is still quite high (~ 200 meV above the Dirac Point). An *in-situ* method that demonstrably tunes E_F would greatly facilitate experiments at the Dirac Point, as proposed in Refs. [1, 2]. Several groups have applied conventional electrostatic gating to tune the chemical potential μ in exfoliated crystals [12–14] and in thin-film samples of Bi_2Se_3 . [15] The newer technique of liquid gating has also been used on Bi-based materials [16–20]. However, in these experiments, SdH oscillations were either not detected at all or poorly resolved. Tuning of the quantum oscillations and showing that they arise from surface Dirac electrons remain to be established.

Here we report that the surface SdH oscillations in $\text{Bi}_2\text{Te}_2\text{Se}$ can be tuned over a broad range using the ionic liquid (DEME-TFSI). In lowering E_F substantially, we access the $N = 1$ Landau level in a magnetic field $B = 14$ T. This allows the $\frac{1}{2}$ -shift characteristic of Dirac electrons to be measured with greatly improved resolution. We find that liquid gating leads to strong enhancement of the mobility μ_s of the surface carriers. Aside from moving E_F closer to the Dirac Point, the tunability yields direct information on the surface and bulk conduction.

As reported earlier [8, 9, 11], the resistance $R(T)$ in $\text{Bi}_2\text{Te}_2\text{Se}$ rises monotonically to very large values as $T \rightarrow 4$ K (curve at $V_G = 0$ in Fig. 1a). Analysis of the Hall

coefficient R_H at 5 K (Fig. 1b) reveals a population of bulk n -type carriers much higher than the population of surface electrons. Nonetheless, a modest, negative gate voltage V_G can increase R by 40% (Fig. 1a) and $|R_H|$ by a factor of 2 at 5 K (Panel b). V_G is applied to the gold electrode (inset in Fig. 1a) at 220 K, and the sample is then cooled below the liquid's glass transition. After the low- T measurements are completed, the sample is warmed to 220 K (at 2 K/min.) and V_G is reset. [21] At 4 K, the large E -field induced by the surface anion density N_{ion} ($1.4 \times 10^{14} \text{ cm}^{-2}$) creates a depletion layer that penetrates deep into the bulk (5–20 μm). [23] As shown in Fig. 1b (inset), the induced upward bending of the bands decreases E_F .

At each value of V_G , the curves of R vs. B display SdH oscillations. To focus on the SdH signal, we have subtracted off a smooth background ρ_B to isolate the oscillatory part of the resistance, $\Delta\rho_{xx} \equiv \rho_{xx} - \rho_B$. Figure 2a displays plots of $\Delta\rho_{xx}$ in Sample 1 versus $1/B$ for 5 values of V_G . The period of the SdH oscillations increases monotonically as V_G changes from 0 to -4.2 V, in accordance with our expectation that E_F is decreasing. Surprisingly, the SdH amplitude is strongly enhanced between $V_G = 0$ and -2.1 V (the former is shown amplified by 5 \times). The dotted curves are the best fits [11] to the Lifshitz-Kosevich (LK) expression for SdH oscillations using only one frequency component. From the fits, we may infer how the surface mobility μ_s changes with V_G (see below). The same trends are evident in Sample 2, which has a higher starting surface density n_s but is taken to $B = 45$ T (Fig. 2b). We find that the SdH oscillations are not resolved at $V_G = 0$, but become prominent at $V_G = -1.5$ V.

In finite B , the surface electronic states are quantized into Landau levels (LLs) with quantum numbers $N = 0, 1, \dots$. The index field B_n is the field at which E_F falls between two LLs. For Schrödinger states, the integer n counts the number of occupied LLs (the highest filled LL has $N_{max} = n - 1$). Using the level degeneracy Be/h per spin, we then have $1/B_n = ne/(hn_s)$ (n_s is the surface density, e the elemental charge and h is Planck's constant).

For Dirac electrons, however, we have $n + \frac{1}{2}$ filled LLs

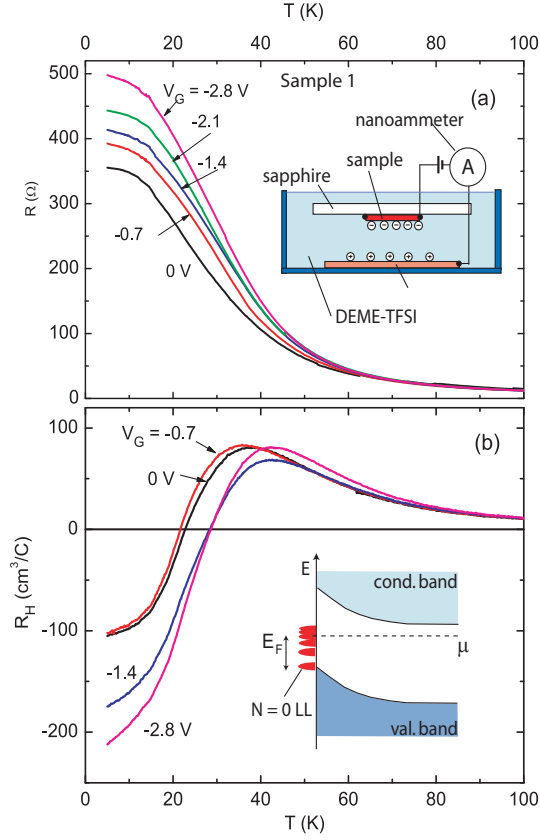


FIG. 1: (color online) The resistance R per square (Panel a) and Hall coefficient R_H vs. T (Panel b) in $\text{Bi}_2\text{Te}_2\text{Se}$ at selected V_G in Sample 1. R_H is measured at fixed B (3 T). Changing V_G from 0 to -2.8 V increases R by 40% and $|R_H|$ by $2\times$. The inset (Panel a) shows the cell housing the sample and the ionic liquid DEME-TFSI. The Au electrode (a circular plate of radius 1.5 mm) is separated by 0.5 mm from the sample. [21] The inset in (b) is a sketch of the band bending induced by liquid gating. Negative ions deposited on the crystal leads to upward band-bending. At the surface, this causes E_F to decrease towards the Dirac Point. LLs are shown as solid half-ovals.

when $B = B_n$ (now $N_{max} = n$). The additional $\frac{1}{2}$ derives from the $N = 0$ LL, or equivalently, from the π -Berry phase intrinsic to each Dirac cone [24]. The relation between $1/B_n$ and n is now $1/B_n = (n + \frac{1}{2})(e/hn_s) - a$ a straight line that intercepts the n -axis at $n = -\frac{1}{2}$. In both cases, G_{xx} is a local minimum at B_n .

If resistivity curves are used, B_n should be identified with the *maxima* in $\Delta\rho_{xx}$. This point is discussed in Refs. [11, 25] In Fig. 3a, we plot as solid symbols B_n in Sample 1 against the integers n (the open symbols corresponding to the minima are plotted against $n + \frac{1}{2}$).

At each V_G , the slope of the straight lines yields the FS area S_F . As $|V_G|$ increases from 0 to 2.8 V, the slopes of the best-fit lines decrease by a factor of 6.4, reflecting a steep decrease in S_F . This decrease saturates when $|V_G|$ exceeds 2.1 V.

In Panel (b), we show the high-field behavior for $|V_G| >$

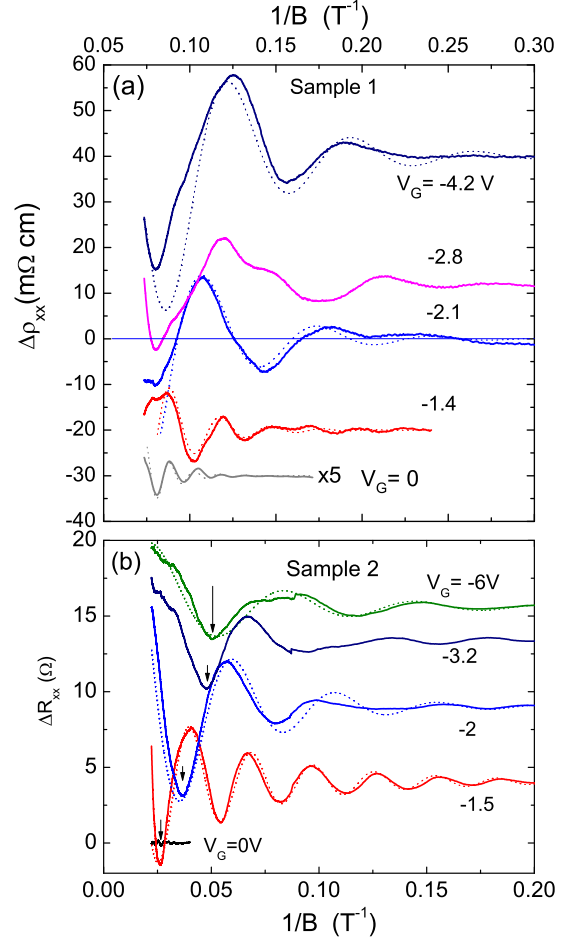


FIG. 2: (color online) Traces of SdH oscillations in the resistance versus $1/B$, showing systematic changes to the oscillation amplitude and period with gate voltage (bold curves, displaced vertically for clarity). The dashed curves are fits to the LK expression with one frequency component [11]. Panel (a) shows traces of $\Delta\rho_{xx}$ vs. $1/B$ at 5 K measured to 14 T for 5 values of V_G (Sample 1) [22]. The largest increase in amplitude occurs between $V_G = 0$ to -1.4 V. The curve at $V_G = 0$ is shown amplified $5\times$. All other curves share the same vertical scale. Panel (b) displays traces of ΔR_{xx} vs. $1/B$ at 0.3 K measured to 45 T at V_G as indicated (Sample 2) [22]. Arrows indicate $n = \frac{1}{2}$ (E_F at center of broadened $N = 1$ LL).

2.1 V in expanded scale. At these large bias values, the intercepts cluster around $n = -\frac{1}{2}$ (-0.46, -0.56 and -0.61). In the corresponding plots for Sample 2 (Panel c), we find that S_F decreases by a factor of 2 between $V_G = -1.4$ and -6 V. In the limit $1/B \rightarrow 0$, the intercepts are at $n = -0.35$, -0.40 and -0.42. In both samples, the last feature observed at the highest B (minima in R_{xx}) corresponds to $n_{min} = \frac{1}{2}$ (this implies that E_F lies in the middle of the broadened $N = 1$ Dirac LL). With such a small n_{min} , we may rigorously exclude an intercept at $n = 0$ in the limit $1/B \rightarrow 0$. [25] Thus the index plots provide rather conclusive evidence that the SdH oscillations arise from surface Dirac electrons.

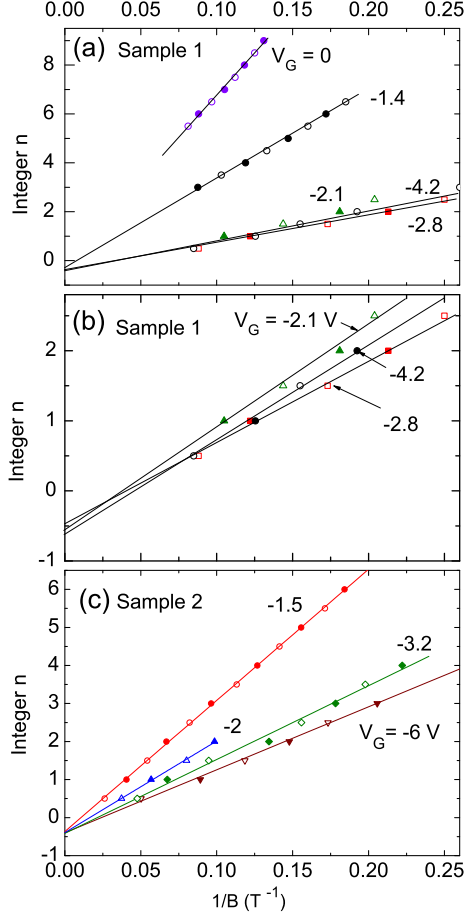


FIG. 3: (color online) Index plots of the integer n vs. $1/B_n$ at selected V_G in Sample 1 (Panels a and b) and 2 (Panel c). Maxima of $\Delta\rho_{xx}$ (solid symbols), corresponding to the index fields B_n , are plotted against n . Minima (open symbols) are plotted against $n + \frac{1}{2}$. Panel (a): As V_G changes from 0 to -2.1 V, the slope of the best fit lines decreases 6-fold. Further increase in $|V_G|$ leads to saturation. In Panel (b), the high-bias curves are displayed in expanded vertical scale. In the limit $1/B \rightarrow 0$, the best-fit lines have intercepts at -0.46, -0.56 and -0.61, consistent with Dirac electrons. The intercepts for Sample 2 (Panel c) also cluster near -0.45 in the limit $1/B \rightarrow 0$.

Returning to Fig. 2, we have fitted the SdH oscillations to the LK expressions (shown as dashed curves). The damping of the oscillations versus B yields the surface mobility μ_s . As shown in Fig. 4b, μ_s in Sample 1 rises from 720 to 2,480 cm²/Vs as $|V_G|$ is increased to 4.2 V. [22] In Fig. 4c, the decrease and eventual saturation in S_F is plotted as a surface density $n_s = k_F^2/(4\pi)$ (per spin). The saturation at large $|V_G|$ either arises from induced chemical reaction or from E_F meeting the top of the valence band. [26]

One figure-of-merit in TI crystals is the ratio of the surface to bulk conductances $\eta \equiv G^s/G^b$ in zero B (with $G^r \equiv G^r_{xx}(0)$, $r = s, b$). In Sample 1, $\eta \sim 0.05$ is quite

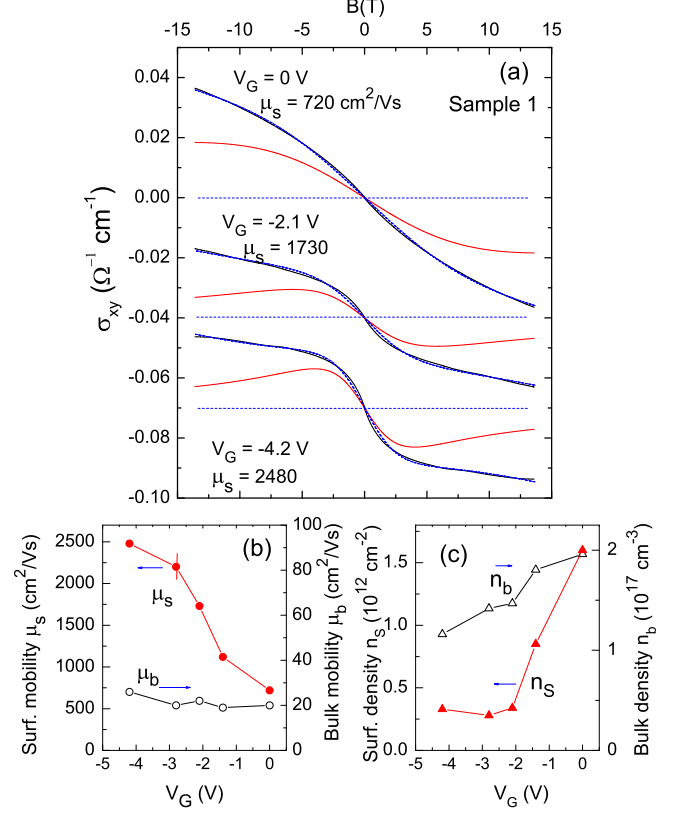


FIG. 4: (color online) Panel (a): The observed Hall conductivity σ_{xy} vs. B in Sample 1, showing weak- B curvature at 3 values of V_G (curves displaced for clarity). At each V_G , the outer curves are the data (solid black curve) and the fit to Eq. 1 (superposed blue dashed curve). The inner (red, solid) curve is the surface term G^s_{xy}/t fixed by n_s and μ_s . (Weak SdH oscillations are apparent in the observed σ_{xy} .) The difference between the outer and inner curves is the bulk term σ^b_{xy} . At $V_G = -4.2$ V, G^s_{xy}/t accounts for 83% of σ_{xy} in weak B . Panel (b) shows that, with increased gating, μ_s increases from 720 to 2,480 cm²/Vs while μ_b stays very small (20-30 cm²/Vs). Panel (c) compares the sharp decrease in n_s with the mild change in n_b with gating. When $|V_G| > 2$ V, n_s saturates.

small (compared with $\eta \sim 1$ obtained in Ref. [9]). However, in the Hall channel, the ratio $\eta_H = G^s_{xy}/G^b_{xy}$ of the surface and bulk conductances (G^s_{xy} and G^b_{xy} , respectively) is enhanced by μ_s/μ_b , which can be very large. We define n_b and μ_b to be the bulk electron density and mobility, respectively, averaged over the whole crystal.

As shown in Fig. 4a, a distinctive feature of σ_{xy} at low T is the curvature in weak B , which grows with increasing $|V_G|$. We may use the semiclassical 2-band expression for σ_{xy} :

$$\sigma_{xy} = n_s e \mu_s \frac{\mu_s B}{t[1 + (\mu_s B)^2]} + n_b e \mu_b^2 B, \quad (1)$$

where the first term is G_{xy}^s/t , with t the thickness ($50\text{ }\mu\text{m}$ in Sample 1). With n_s and μ_s fixed by analysis of the SdH oscillations, this term is non-adjustable. The second term is the bulk Hall conductivity σ_{xy}^b in the low-mobility limit. With the sole adjustable parameter $P_b \equiv n_b\mu_b^2$, we find that Eq. 1 gives a very good fit (dashed curves). For comparison, we have also plotted G_{xy}^s/t (inner, faint solid curves). Combining P_b with the zero- B value of σ_{xx}^b , we finally obtain n_b and μ_b separately for each value of V_G . These are reported in Figs. 4b and 4c. The small values of μ_b ($20\text{--}30\text{ cm}^2/\text{Vs}$) result in a large $\mu_s/\mu_b \sim 100$ and $\eta_H \sim 5$. This accounts for the pronounced low- B curvatures seen in Fig. 4.

The analysis implies high-mobility Dirac electrons in parallel with a much larger population of bulk electrons. Because of the 100-fold difference in mobilities, the Dirac electrons produce 83% of the total weak- B Hall conductance at large $|V_G|$. The fits include the surface Hall conductance from only one surface. Since its G_{xy}^s already accounts for most of the observed σ_{xy} , there is very little room left for a second surface term. We estimate that the Hall contribution from the other surface is less than 2% of σ_{xy} , which implies that its μ_s is $<300\text{ cm}^2/\text{Vs}$. This cannot produce resolvable SdH oscillations.

The large enhancement of μ_s by liquid gating (Fig. 4b)

is perhaps the most intriguing feature reported here. To our knowledge, this is the first realization of enhancement of surface SdH amplitudes by an *in situ* technique. [27] A recent STM experiment [28] reveals that the Dirac Point closely follows spatial fluctuations of the local potential on length scales of $30\text{--}50\text{ nm}$. This could lead to strong scattering of surface electrons. We speculate that, under liquid gating, the anions accumulate at local maxima in the potential, thereby levelling out the strongest spatial fluctuations. [29] The results provide encouragement that alternative routes that even out local potential fluctuations can lead to further improvements in μ_s .

We thank Joe Checkelsky, Jianting Ye, and Hongtao Yuan for advice on liquid gating. The research is supported by the US National Science Foundation (Grant No. DMR 0819860) and the Army Research Office (ARO W911NF-11-1-0379). Sample growth and characterization were supported by an award from the Defense Advanced Research Projects Agency under SPAWAR Grant No. N66001-11-1-4110. High-field measurements were performed at the National High Magnetic Field Laboratory which is supported by NSF (Award DMR-084173), by the State of Florida, and by the Department of Energy.

-
- [1] M. Z. Hasan and C. L. Kane, Rev. Mod. Phys. **82**, 3045 (2010).
 - [2] Xiao-Liang Qi and Shou-Cheng Zhang, Rev. Mod. Phys. **83**, 1057 (2010).
 - [3] D. Hsieh, D. Qian, L. Wray, Y. Xia, and Y. S. Hor, R. J. Cava, and M. Z. Hasan, Nature (London) **452**, 970 (2008).
 - [4] P. Roushan, J. Seo, C. V. Parker, Y. S. Hor, D. Hsieh, D. Qian, A. Richardella, M. Z. Hasan, R. J. Cava, and A. Yazdani, Nature (London) **460**, 1106 (2009).
 - [5] Dong-Xia Qu, Y. S. Hor, Jun Xiong, R. J. Cava, and N. P. Ong, Science **329**, 821 (2010).
 - [6] James G. Analytis, Ross D. McDonald, Scott C. Riggs, Jiun-Haw Chu, G. S. Boebinger and Ian R. Fisher, Nature Physics **6**, 960 (2010).
 - [7] Hailin Peng, *et al.*, Nature Materials **9**, 225-229 (2009).
 - [8] Zhi Ren, A. A. Taskin, Satoshi Sasaki, Kouji Segawa and Yoichi Ando, Phys. Rev. B **82**, 241306(R) (2010).
 - [9] Jun Xiong, A.C. Petersen, Dongxia Qu, Y.S. Hor, R. J. Cava, N.P. Ong, Physica E **44**, 917 (2012).
 - [10] S. Jia, H.W. Ji, E. Climent-Pascual, M. K. Fuccillo, M. E. Charles, J. Xiong, N. P. Ong, and R. J. Cava, Phys. Rev. B **84**, 235206 (2011).
 - [11] Jun Xiong, Yongkang Luo, YueHaw Khoo, Shuang Jia, R. J. Cava, and N. P. Ong, Phys. Rev. B **86**, 045314 (2012).
 - [12] J. G. Checkelsky, Y. S. Hor, R. J. Cava, and N. P. Ong, Phys. Rev. Lett. **106**, 196801 (2011).
 - [13] Hadar Steinberg, Dillon R. Gardner, Young S. Lee, and Pablo Jarillo-Herrero, Nano Lett. **10**, 5032 (2010).
 - [14] Benjamin Sacepe, Jeroen B. Oostinga, Jian Li, Alberto Ubaldini, Nuno J.G. Couto, Enrico Giannini and Alberto F. Morpurgo, Nature Communications **2**, 575 (2011).
 - [15] H. Steinberg, J.-B. Laloe, V. Fatemi, J. S. Moodera and P. Jarillo-Herrero, Phys. Rev. B **84**, 233101 (2011).
 - [16] Hongtao Yuan, Hongwen Liu, Hidekazu Shimotani, Hua Guo, Mingwei Chen, Qikun Xue and Yoshihiro Iwasa, Nano Lett. **11**, 2601 (2011).
 - [17] Dohun Kim, Sungjae Cho, Nicholas P. Butch, Paul Syers, Kevin Kirshenbaum, Shaffique Adam, Johnpierre Paglione and Michael S. Fuhrer, Nature Physics **8**, 459 (2012).
 - [18] Joseph G. Checkelsky, Jianting Ye, Yoshinori Onose, Yoshihiro Iwasa and Yoshinori Tokura, Nature Physics **8**, 729 (2012).
 - [19] Sunao Shimizu, Ryutaro Yoshimi, Takafumi Hatano, Kei S. Takahashi, Atsushi Tsukazaki, Masashi Kawasaki, Yoshihiro Iwasa, and Yoshinori Tokura, Phys. Rev. B **86**, 045319 (2012).
 - [20] Kouji Segawa, Zhi Ren, Satoshi Sasaki, Tetsuya Tsuda, Susumu Kuwabata, and Yoichi Ando, Phys. Rev. B **86**, 075306 (2012).
 - [21] In our experiment, the sample is immersed in the ionic liquid DEME-TFSI, comprised of cations $(\text{CH}_3\text{CH}_2)_2(\text{CH}_2\text{CH}_2\text{OCH}_3)\text{CH}_3\text{N}^+$ and anions $(\text{CF}_3\text{SO}_2)_2\text{N}^-$. The liquid is pumped at 25°C for 2 hours prior to application to minimize water content. Liquid gating has several pitfalls when used on crystals. The stresses induced by repeated freezing and thawing of the ionic liquid can snap the leads or the crystal itself. Also, a large $|V_G|$ can trigger an electrical discharge which invariably leads to a steep collapse of R (at 5 K). Unlike in thin films, changes to R with V_G are not resolved above $\sim 100\text{ K}$ (see Fig. 1a). To minimize sample

- damage, we start at $V_G = 0$ followed by measurements at increasingly negative V_G until the sample fails (usually by a discharge event). At 220 K, V_G is changed in steps of -0.1 V, while monitoring the transient current I_{tr} (1-40 nA). The time spent at 220 K is under 30 s. On returning V_G to 0, we recover the same starting value of R (at 5 K) provided $|V_G|$ is kept below ~ 2 V.
- [22] The crystal dimensions of Sample 1 are $0.9 \times 0.75 \times 0.05$ mm³. For Sample 2, they are $1.35 \times 0.61 \times 0.026$ mm³. In Sample 2, the steepest change in μ_s occurs between $V_G = 0$ and -1.5 V, at which $\mu_s = 2,800$ cm²/Vs. At larger gate, it saturates ($\mu_s = 3,000$ cm²/Vs at -6 V).
- [23] We estimate the depletion width d as follows. From n_b at 4 K, we estimate the donor concentration $N_d \sim 2 \times 10^{17}$ cm⁻³. Integrating the transient current, $\int_0^t I_{tr}(t') dt'$, we obtain the surface anion density $N_{ion} = 1 - 4 \times 10^{14}$ (for $|V_G| < 2$ V). To screen the intense E field produced, we need a depletion layer of width $d \simeq N_{ion}/N_d \simeq 5-20$ μ m (screening by the surface electrons is negligible). This is consistent with the 2-fold increase in R_H at large $|V_G|$.
- [24] Yuanbo Zhang, Yan-Wen Tan, Horst L. Stormer and Philip Kim, Nature **438**, 201 (2005).
- [25] In general, it is best to convert the resistivity tensor R_{ij} to the conductance tensor G_{ij} , and to identify B_n with the minima in G_{xx} . However, in many experiments (two-terminal measurements or experiments on nanowires), the Hall resistance R_{yx} is unavailable. Because the total conductance in Bi-based TI systems is dominated by low-mobility bulk electrons, we have $|R_{yx}| \ll R_{xx}$. Then R_{xx} has a local maximum whenever G_{xx} has a local minimum, and we should identify B_n with the fields at which R_{xx} attains local *maxima*. The wrong assignment (identifying B_n with minima in R_{xx}) shifts the intercept by $\pm \frac{1}{2}$. This leads to mis-identifying the SdH oscillations from bulk carriers as arising from Dirac electrons.
- [26] The possibility that the strong E -field can induce chemical doping of the sample is an important concern in liquid-gating experiments. Our results suggest that electrostatic gating is the dominant effect at small values of $|V_G|$, and chemically induced doping is important only when $|V_G|$ exceeds roughly 2 V. As evident in Figs. 4b and 4c, the rapid changes in n_s and μ_s occur for $|V_G| < 2$ V. In more extensive tests (on Samples 3,4), we find that changes to both R and R_H observed at 5 k are reversible over this restricted range of V_G (i.e. they recover their starting values within 2% when V_G is returned to 0). This reversibility suggests that the changes are caused by reversible bending of the band, i.e. gating. Moreover, the strong enhancement of μ_s is incompatible with chemical doping, which should introduce increased scattering of the surface electrons. When $|V_G|$ exceeds 2 V, however, R and R_H become hysteretic as V_G is cycled. This suggests that chemical doping becomes increasingly dominant. It is suggestive that the saturation in n_s observed for $|V_G| > 2$ V (Fig. 4b) may signal the onset of strong chemical doping. However, other causes, e.g. E_F touching the bulk valence band maximum, cannot be excluded at present. This issue is under active investigation.
- [27] Previous gating experiments reported either a decrease in μ_s with finite gating [17], or a non-monotonic variation of μ_s that trends downwards with increasing $|V_G|$ [20]. SdH oscillations were not resolved in these studies.
- [28] Haim Beidenkopf, Pedram Roushan, Jungpil Seo, Lindsay Gorman, Ilya Drozdov, Yew San Hor, R. J. Cava, and Ali Yazdani, Nature Physics **7**, 939 (2011).
- [29] Enhancement in μ_s could also result from separation of the surface and bulk electrons by the depletion layer, if Coulomb interaction is large.